CrossMark

ORIGINAL ARTICLE

Aligned ovine diaphragmatic myoblasts overexpressing human connexin-43 seeded on poly (L-lactic acid) scaffolds for potential use in cardiac regeneration

Carlos Sebastián Giménez · Paola Locatelli · Florencia Montini Ballarin · Alejandro Orlowski ·
Ricardo A. Dewey · Milagros Pena · Gustavo Abel Abraham · Ernesto Alejandro Aiello ·
María del Rosario Bauzá · Luis Cuniberti · Fernanda Daniela Olea · Alberto Crottogini

Abstract Diaphragmatic myoblasts (DMs) are precursors of type-1 muscle cells displaying high exhaustion threshold on account that they contract and relax 20 times/min over a lifespan, making them potentially useful in cardiac regeneration strategies. Besides, it has been shown that biomaterials for stem cell delivery improve cell retention and viability in the target organ. In the present study, we aimed at developing a novel approach based on the use of poly (L-lactic acid) (PLLA) scaffolds seeded with DMs overexpressing connexin-43 (cx43), a gap junction protein that promotes inter-cell connectivity. DMs isolated from ovine diaphragm biopsies were characterized by immunohistochemistry and ability to differentiate into myotubes (MTs) and transduced with a lentiviral vector encoding cx43. After confirming cx43 expression (RT-qPCR and Western blot) and its effect on inter-cell connectivity (fluorescence recovery after photobleaching), DMs were grown on fiber-aligned or random PLLA scaffolds. DMs were successfully isolated and characterized. Cx43 mRNA and protein were overexpressed and favored inter-cell connectivity. Alignment of the scaffold fibers not only aligned but also elongated the cells, increasing the contact surface between them. This novel approach is feasible and combines the advantages of bioresorbable scaffolds as delivery method and a cell type that on account of its features may be suitable for cardiac regeneration. Future studies on animal models of myocardial infarction are needed to establish its usefulness on scar reduction and cardiac function.

C. S. Giménez (✉) · P. Locatelli · María del RosarioBauzá · L. Cuniberti · F. D. Olea · A. Crottogini
Instituto de Medicina Traslacional, Transplante y Bioingeniería (IMETTYB), Universidad Favaloro-CONICET, Solís 453, C1078AAI Buenos Aires, Argentina
e-mail: sgimenez@favaloro.edu.ar

F. Montini Ballarin · G. A. Abraham
Instituto de Investigaciones en Ciencia y Tecnología de Materiales (INTEMA), Universidad Nacional de Mar del Plata-CONICET, Mar del Plata, Argentina

A. Orlowski
Centro de Investigaciones Cardiológicas (CIC), Universidad Nacional de La Plata-CONICET, La Plata, Argentina

R. A. Dewey · M. Pena · E. A. Aiello
Instituto de Investigaciones Biotecnológicas-Instituto Tecnológico de Chascomús (IIB-INTECH), Universidad Nacional de San Martín-CONICET, Chascomús, Argentina

Introduction

One of the main challenges in regenerative medicine is reducing myocardial infarct size, to avoid or minimize the post-infarction ventricular remodeling process that leads to heart failure (Sutton and Sharpe 2000).

One of the stem cell-based strategies that have been used to this end is implanting skeletal myoblasts into infarction scars. Despite some positive results were observed (Menasché et al. 2003; Dib et al. 2005), life-threatening arrhythmias have been reported in clinical trials (Siminiak et al. 2004; Fernandes et al. 2006; Menasché et al. 2008). This has been attributed to down-regulation of connexin-43 (cx43) expression in myoblasts undergoing differentiation into myotubes (MTs). Cx43 is a member of the connexin family that forms gap junctions between adjacent cells, its downregulation preventing inter-cell connectivity and beating synchrony with resident cardiomyocytes (Suzuki et al. 2001; Abraham et al. 2005; Delmar and Makita 2012).

Importantly, the muscle type from which the cells are harvested has rarely been taken into consideration. Skeletal muscles differ not only in function, but also in the type of fiber sub-populations and metabolic properties. It has been shown that skeletal myoblasts display large heterogeneity in terms of proliferation, fusion capacity and ability to differentiate into diverse cell lineages (Baroffio et al. 1995; Beauchamp et al. 1999; Redshaw et al. 2010). In this regard, diaphragmatic myoblasts (DMs) may be a good option, not only because its fibers are type 1, but also because they display a much higher exhaustion threshold, on account that they contract and relax 20 times per minute over a lifetime. However, to our knowledge, diaphragmatic myoblasts have not been used in studies of cardiac regeneration.

On the other hand, it has been reported that bioengineered constructs such as bioresorbable scaffolds, may either induce cardiac regeneration by themselves, or act as delivery systems of cells grown on them (Liu et al. 2015). In this regard, synthetic polyesters such as poly (L-lactic acid) (PLLA) offer a number of advantages over other materials for developing scaffolds in tissue engineering. PLLA is a FDA-approved biomaterial with high strength and elastic modulus, good processability and electrospinnability. It is commonly used in biomedical applications such as bioresorbable implants, sutures, drug delivery systems, tissue engineering, and medical devices (Gupta et al. 2007; Lopes et al. 2012).

Electrospinning is a versatile processing technology to produce scaffolds with random or aligned nanofibers, high porosity and high surface-to-volume ratio able to mimic the extracellular matrix morphology. Furthermore, it allows adjustment of processing parameters to obtain nanofibrous scaffolds with tunable orientation, pore and nanofiber diameter (Yarin and Zussman, 2004; Reneker et al. 2007; Kai et al. 2013). These properties also influence the response of cells in contact with the scaffold and with the tissue (Beachley and Wen 2010; He et al. 2014).

The aim of this work was to isolate, culture and characterize ovine DMs, transduce them with a lentiviral vector encoding human cx43 to induce connection between cells, and finally grow them on scaffolds made from aligned electrospun PLLA nanofibers, to generate DMs-carrying sheets for later testing in ovine models of myocardial infarction and heart failure.

Materials and methods

All procedures were carried out in accordance with the Guide for Care and Use of Laboratory Animals, published by the U.S. National Institutes of Health (NIH Publication No. 85–23, revised 1996) and approved by the Laboratory Animal Care and Use Committee (CICUAL) of the Favaloro University (approval #DCT0153-12).

Obtention of a feeder layer of autologous macrophages

Seven days previous to diaphragm extraction, 20 cm^3 of blood were obtained from each sheep's antecubital vein in order to construct a feeder layer of autologous macrophages, as previously reported (Sepúlveda et al. 2016). This feeder layer was employed only for the primary culture of DMs but was not needed after the first passage. Briefly, the blood sample was diluted in the same volume of PBS buffer (Gibco, Grand Island, NY, USA) and processed with Ficoll-Paque (GE Healthcare, Uppsala, Sweden). The cell layer containing peripheral blood monocytes was isolated. Cells were plated and the adherent ones were

incubated at 37 °C and 5% CO_2 in high-glucose Dulbecco's modified Eagle medium (DMEM, Gibco) supplemented with 2% (v/v) antibiotic–antimycotic (Anti–Anti, Gibco), 20% (v/v) fetal bovine serum (FBS, NATACOR, Buenos Aires, Argentina). Cells were fed every 72 h and characterized by anti-CD68 antibody (ab31630 Abcam, Cambridge, MA, USA) (supplementary Fig. 1A–B).

Diaphragm extraction

Four male Corriedale sheep weighing 30–40 kg were premedicated with acepromazine maleate (Holliday-Scott S.A., Béccar, Argentina) 0.3 mg/kg. Anesthesia was induced with intravenous propofol (Fresenius Kabi Austria GmbH, Graz, Austria) 3 mg/kg and maintained with 2% isoflurane (Piramal Critical Care Inc., Bethlehem, PA, USA) in oxygen under mechanical ventilation (Servo 900C, Siemens, Solna, Sweden). A sterile mini-thoracotomy was performed at the right fourth intercostal space. A 4 cm surgical incision was performed in the aponeurosis of the diaphragm muscle to obtain a 1–2 cm^2 sample of the diaphragm. Subsequently, the aponeurosis was sutured and the thoracotomy repaired. Sheep were returned to the animal house under analgesic treatment (supplementary Fig. 1C–E).

Isolation, culture and differentiation of ovine DMs

Diaphragm samples were rinsed several times with PBS. After mechanically removing the connective tissue, the remaining tissue was fragmented in 2 mm^2 pieces, which were treated with Collagenase V (Sigma-Aldrich, St. Louis, MO, USA) to obtain DMs. The cells were rinsed, centrifuged several times and cultured for 2 h at 37 °C to allow for DMs purification through sedimentation. Finally, a primary culture of DMs was obtained by seeding the DM-containing supernatant on the feeder layer of autologous macrophages. As stated above, this feeder layer was no longer used in subsequent passages.

DMs were induced to differentiate into MTs. To this end, DMs cultures exhibiting 90–100% confluence were incubated in high-glucose DMEM supplemented with 2% FBS and 2% antibiotic–antimycotic at 37 °C and 5% CO_2, until myotube formation was observed.

Immunocytochemistry

Cultures at passages 2–4 and 60–80% confluence were used for cell characterization. For immunostaining, the medium was carefully removed, cells were rinsed with PBS and fixed in methanol for 10 min. Cells were then rinsed 3 times with PBS and 3 min with Super Sensitive TM Wash Buffer (BioGenex, Fremont, CA, USA). Fixed cells were incubated with Protein Block (BioGenex), then rinsed with Wash Buffer and incubated with primary antibodies. The primary antibodies employed were anti-CD68 (ab31630, Abcam), anti-desmin (PA0032, Leica, Newcastle upon Tyne, UK), anti α-sarcomeric actin (A2172, Sigma-Aldrich), anti SERCA-2 ATPse (ab77289, Abcam), anti-MyoD (sc-377186, Santa Cruz Biotech., Santa Cruz, CA, USA), anti-fast myosin skeletal heavy chain (MHC) (ab75370, Abcam), and anti-cx43 (sc-101660, Santa Cruz). After incubation with the primary antibody, cell monolayers were post-incubated with SS Multilink (BioGenex), post-treated with fluorescein-avidin or Texas red-avidin (Vector Labs, Peterborough, UK). After nuclear staining with DAPI, cells were examined with a fluorescence microscope (Axiophot, Zeiss, Jena, Germany) with the aid of a computer-assisted image-analysis program (Zeiss AxioCam MRc5 camera and AxioVision software, Carl Zeiss Thornwood, NY, USA).

Lentiviral vectors

Cell-free third-generation lentiviral vectors (Lv) were generated by the calcium phosphate co-transfection method of 293T cells with either pCMV/EGFP (encoding green fluorescent protein) or pCMV/CX43iresGFP (encoding both connexin 43 and green fluorescent protein), and the packaging constructs pMDLg/pRRE, pRSV-REV, and pCMV-VSVG in the presence of cloroquine (Sigma-Aldrich). Viral titers were determined on A549 cells by flow cytometry (FACSCalibur, BD Biosciences, Franklin Lakes, NJ, USA), yielding vector titers of 10^6–10^8 TU (transducing units)/ml.

DMs transduction

With the objective of assessing the efficiency of transduction (ET), DMs were transduced with Lv.

pCMV/EGFP vectors at 0, 25, 50, 100 and 200 virions particles per cell (MOI: multiplicities of infection) for 72 h at 37 °C and 5% CO_2, in high-glucose DMEM supplemented with 20% FBS and 2% antibiotic–antimycotic, in the presence of 8 µg/ml polybrene (Sigma-Aldrich). DMs overexpressing GFP were obtained and the ET for different MOI was assessed by flow cytometry using FL1-H (green fluorescence detector) and FSC-H (forward scatter detector). ET was reported as percentage of number of green fluorescents cells. The baseline green fluorescence emission was set with DMs (MOI = 0). The MOI selected was used to transduce DMs with Lv.pCMV/CX43ires GFP vector (DMcx43) at the same conditions.

RT-qPCR

For gene expression analysis of cx43, frozen DMs and MTs with and without transduction were homogenized in Trizol reagent (Life Technologies, Carlsbad, CA, USA) according to the manufacturer's instructions for total RNA isolation. Then, we treated the samples with DNAsaI (Promega, Fitchburg, WI, USA) and we performed reverse-transcription for cDNA obtention (High capacity cDNA reverse transcripase kit, Applied Biosystems, Foster City, CA, USA) following manufacturer´s protocols. Expression of human cx43 was assessed by real time PCR (StepOne Real-Time PCR System, Applied Biosystems) with SYBR® Select Master Mix reagent (Applied Biosystems). The threshold cycle (Ct) values were determined and normalized to GAPDH in order to adjust for equal amounts of RNA. Forward and reverse primers used in this assay were: CX43 forward: 5′CAAGTGAGCAAAACTGGGCTA A 3′, reverse: 5′CGCCTGCCCCATTCG 3′; GAPDH: forward: 5′ TCTTCCAGGAGCGAGATC C3′, reverse: 5′TGAGCCCCAGCCTTCTCC 3′. All primers were designed using Primer Express software (V3.0, Applied Biosystems).

Western Blot

Cell lysates were washed with PBS and prepared by addition of SDS-PAGE sample buffer [20% (vol/vol) glycerol, 2% (vol/vol) 2-mercaptoethanol, 4% (wt/vol) SDS, 1% (wt/vol) bromophenol blue, 150 mM Tris, pH 6.8]. Before analysis, samples were sheared

through a 26-gauge needle and heated at 80 °C for 5 min. Samples were resolved by SDS-PAGE on 12% acrylamide gels. Proteins were transferred to polyvinylidene difluoride (PVDF) membranes by electrophoresis for 1 h at 100 V at room temperature, in buffer composed of 20% (vol/vol) methanol, 25 mM Tris, and 192 mM glycine. PVDF membranes were blocked by incubation for 1 h in TBST-M buffer [TBST buffer 0.1% (vol/vol) Tween 20, 137 mM NaCl, 20 mM Tris, pH 7.5], containing 10% (wt/vol) nonfat dry milk and then incubated overnight in 10 ml TBST-M [5% (wt/vol) nonfat dry milk], containing rabbit anti-cx43 antibody (1:1.000 dilution). Blots were incubated for 1 h with 10 ml TBST-M containing donkey anti-rabbit IgG conjugated with horseradish peroxidase (sc-2313, Santa Cruz). Blots were visualized and quantified, using ECL reagent and a Chemidoc Image Station (Bio-Rad, Richmond, CA, USA). Bands were densitometry quantified using the software ImageJ (National Institutes of Health, Bethesda, MD, USA). Total protein bands were normalized to corresponding actin (ab8227, Abcam) band density (used as a loading control).

Fluorescence recovery after photobleaching (FRAP)

DMs and DMcx43 were plated in 35 mm Petri dishes using the same culture conditions described above. Cells were stained with 5 µg/ml Calcein Red–Orange AM (ThermoFisher, cat: C34851) for 30 min at 37 °C, and then washed with HEPES buffer (133 mM NaCl, 5 mM KCl, 1.2 mM $MgSO_4$, 0.8 mM $MgCl_2$, 10 mM glucose, 1.35 mM $CaCl_2$ and 10 mM HEPES; pH = 7.35). Images were acquired in HEPES buffer at room temperature using a confocal microscope (Leica TCS SP5 spectral, Wetzlar, Germany) and a 10× objective. GFP-expressing cells were selected in order to perform FRAP experiments. One image was acquired before photobleaching to establish baseline fluorescence intensity in cells stained with Calcein Red–Orange AM (577 nm excitation/590 nm emission). The bleaching plane was set and a region of interest (RoI) was drawn around one cell. RoI was photobleached through excitation with the Helio-Neon laser at 543 nm and 1.5 mW/cm^2 for 60 cycles, resulting in a bleaching time of 236.5 s. After photobleaching, 15 images were acquired every 60 s,

with a scan time of 3.87 s per image and an image size of 512 × 512 pixels.

For analysis of dye diffusion after photobleaching, image processing and analysis of fluorescence intensity in a RoI were accomplished using ImageJ. Fluorescence intensity values were averaged for bleached areas of different individual cells. In general, fluorescence intensity sharply decreased immediately after photobleaching and increased following an inverse exponential function:

$$I(t) = \left(I_\infty - I_p\right)\left(1 - e^{-kt}\right) + I_p$$

where I(t) is the normalized fluorescence intensity, I_p is the theoretical fluorescence intensity immediately after bleaching, I_∞ is the asymptotic theoretical maximal recovery, and k is the recovery rate. The recovery rate (k) was calculated by plotting $[-\ln(1 - F(t)]$ versus (time) resulting in a straight line with a slope equal to k (Lee et al. 2011; Farnsworth et al. 2014).

Electrospinning of aligned poly (L-lactic acid) (PLLA) scaffolds

We employed PLLA (PLA2002D, Mn 78.02 kg/mol, Mw 129.91 kg/mol, IP 1.67) from Natureworks (Minnetonka, MN, USA); dichloromethane (DCM) and N,Ndimethylformamide (DMF) (Sigma-Aldrich). PLLA solutions in DCM:DMF (60:40 v/v) were prepared to have 10% w/v PLLA. Intrinsic solution properties and setup parameters were optimized in previous work to obtain bead-free fibrous scaffolds (Montini Ballarin et al. 2014). A classic flat collector was used to obtain random electrospun membranes (Voltage, ΔV = 10 kV; needle-collector distance, d = 10 cm; flow rate, f = 0.5 ml/h). In this work, aligned scaffolds were optimized using a 20 cm diameter rotating drum as collector system (YFLOW Electrospinning unit 2.2.D-350, Málaga, Spain) and same previously optimized parameters. In order to attract the fibers to the rotating collector, a negative voltage (− 3 kV) was applied to the collector, and a positive tension of 10 kV was applied to the needle tip. Different rotation speeds were tested to optimize the fiber alignment [r = 600 (r1), 950 (r2) and 1175 rpm (r3)]. All experiments were carried out at room temperature in a chamber having a ventilation system with controlled temperature and humidity.

The electrospun scaffolds were dried under vacuum at room temperature to fully eliminate the residual solvent, and finally stored in a desiccator.

Scaffold characterization

Micrographs of the PLLA scaffolds (after sputter coating with gold) were recorded in a scanning electron microscope (JSM-6460LV, JEOL, Akishima, Tokyo, Japan). Diameter and orientation of 200 nanofibers per sample were measured and processed using Image-Pro Plus software (Media Cybernetics). Differential Scanning Calorimetry (DSC) analyses were carried out with a Pyris 1 instrument (Perkin-Elmer, Shelton, CT, USA), heating at 10 °C/min from 0 to 200 °C under nitrogen atmosphere, and glass transition, crystallization and melting events characterized. Crystallinity was estimated from melting and crystallization enthalpies calculated taking into account the PLLA 100% crystalline melting enthalpy.

Cells orientation

DMcx43 stained with PKH26 (Sigma-Aldrich) were seeded on aligned and random nanofiber PLLA scaffolds for 4 days in the culture conditions described above. Confocal micrographs were also processed with Image-Pro Plus software to obtain orientation histograms, mean angle and standard deviation. At least 100 cells per sample were measured. On the oriented scaffolds, the predominant direction of the scaffold nanofibers was used as normalizing parameter of the angle measurements.

Viability

We assessed whether the interventions applied to the cells, namely the genetic modification and their growth on aligned PLLA scaffolds affected cell viability. To this end, we used MTS (n = 4, triplicates) following the manufacturer's instructions (Cell Titer 96 wells Aqueous non-Radioactive Cell Proliferation Assay; Promega), to compare cell viability of: (1) DMcx43 (MOI = 100) vs. DMs (non-transduced) grown on glass disks used as ordinary cell culture surface, and (2) DMs and DMcx43 grown on aligned PLLA scaffolds versus grown on glass disks. The percentages of viability reported were relative to DM

(non-transduced) cultured on glass disks surface during 4 days at 37 °C and 5% CO_2, in high-glucose DMEM supplemented with 20% FBS and 2% antibiotic–antimycotic.

Statistical analysis

All results are expressed as mean $\pm$ SD unless otherwise stated. Student's t tests or 1-way ANOVA-Bonferroni were used to compare the different groups using GraphPad Prism software (version 5.0; Graph-Pad Software Inc., La Jolla, CA, USA). Statistical significance was set at $p < 0.05$.

Results

Isolation, culture and characterization of DMs

Diaphragm satellite cells were successfully isolated from diaphragm biopsies. Neither surgical nor postoperative complications occurred. After 1 week culture, we observed the first cells with a DM phenotype (Fig. 1a). After passage 2–5, we only found cells with the myoblast-specific phenotype that were positive for desmin, sarcomeric α-actin and SERCA2 ATPase (Fig. 1b–d). This was confirmed by their ability to differentiate into MTs (Fig. 1e). Figure 1f, g shows MTs that stain positive for MyoD, a specific factor taking part in the myogenic process, and skeletal muscle myosin heavy chain, respectively.

Connexin-43 overexpression in DMs

Figure 2a shows the lentiviral vectors used. We selected the MOI 100 because it yielded an ET of 70.82% (Fig. 2b). Although an MOI 200 increased TE to 79%, we did not consider that this increase justified duplicating the viral load of the cells. Figure 2c shows DMs transduced with Lv.pCMV/EGFP at MOI 100.

DMs transduced with the vector Lv.pCMV/CX43iresGFP showed a significant increase in the
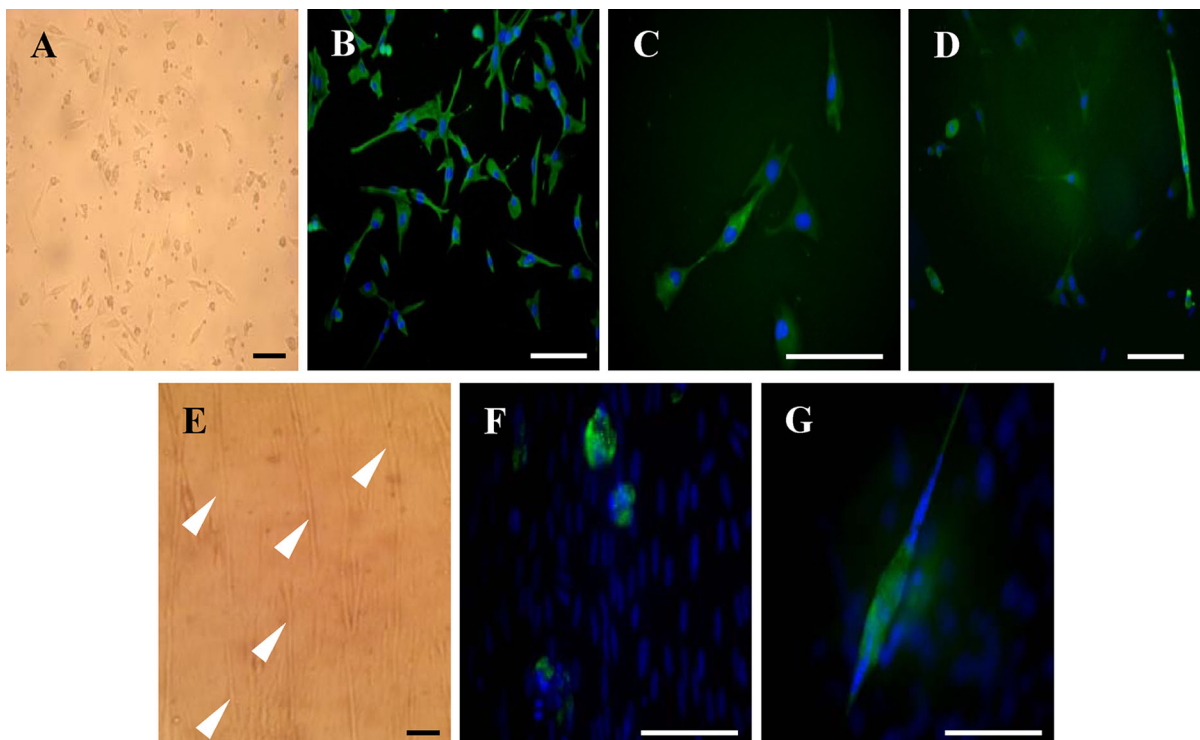
Fig. 1 Characterization of diaphragmatic myoblasts. **a** Isolated diaphragmatic myoblasts cultured on a feeder layer of autologous macrophages. **b–d** Green fluorescence immunostaining for desmin (**b**), sarcomeric α-actin (**c**) and SERCA 2 ATPase (**d**) in cultured diaphragmatic myoblasts. Nuclei are stained blue (DAPI). **e** Arrow heads show diaphragmatic myoblasts differentiated into myotubes. **f, g** Green fluorescence immunostaining for MyoD (**f**) and skeletal muscle myosin heavy chain (**g**) in cultured myotubes. Bars: 50 μm
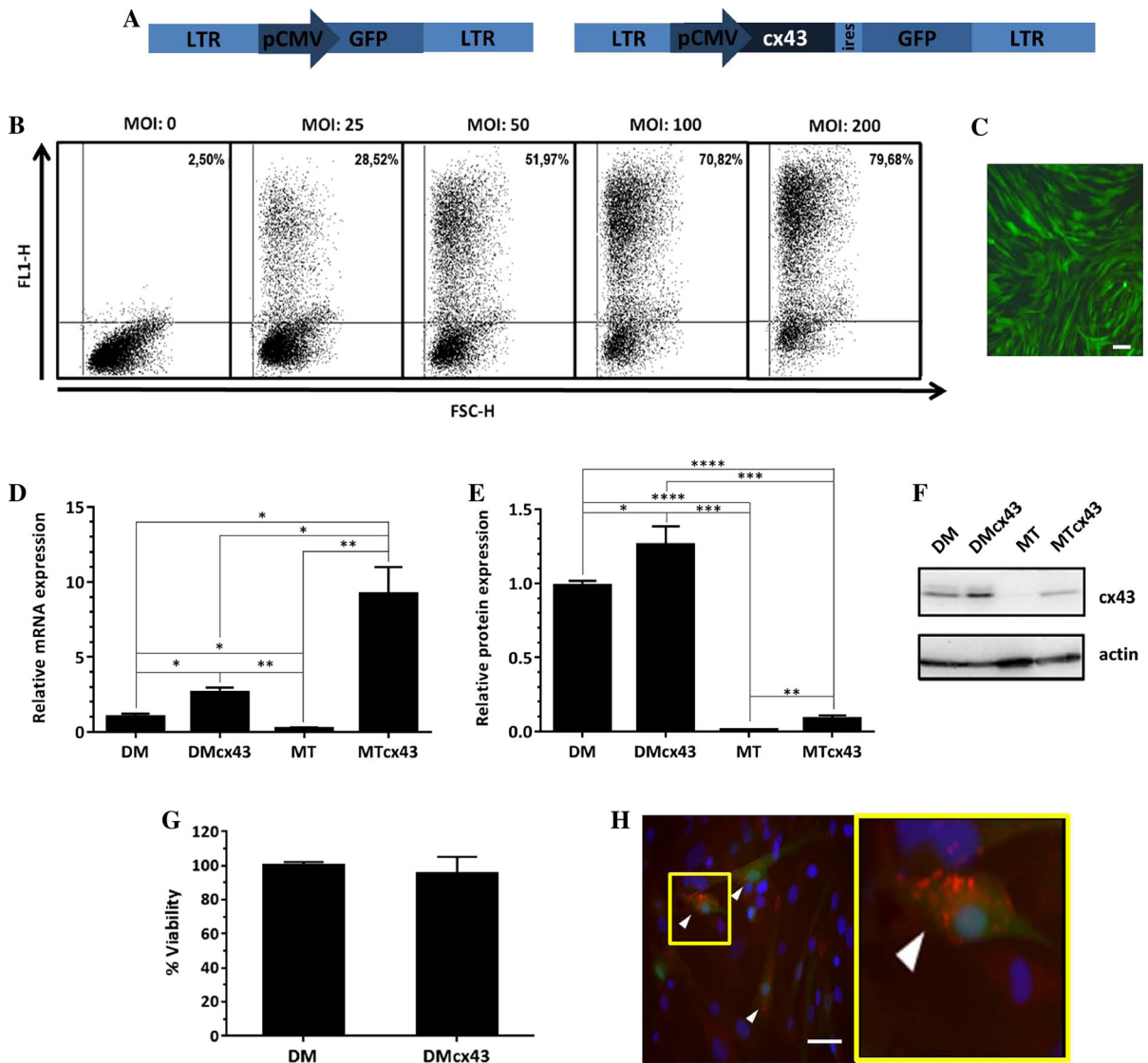
Fig. 2 Connexin-43 overexpression. a Developed lentiviral vectors (left: pCMV/EGFP; right: pCMV/CX43iresGFP). b Transduction efficiency for different multiplicities of infection (MOI) using flow cytometry; y-axis: FL1-H (green fluorescence detector), x-axis: FSC-H (forward scatter detector). c Diaphragmatic myoblasts transduced with MOI = 100 and expression of GFP in the cells. d mRNA levels of connexin-43 (* $p < 0.05$; ** $p < 0.01$; *** $p < 0.001$; **** $p < 0.0001$; one way ANOVA-Bonferroni). e Western blot quantification of connexin-43 protein. f Representative image of Western blot membranes g Percent cell viability assessed by MTS assay ($p = $ NS, unpaired t-test). h Immunostaining (red: anti-human connexin-43; green: GFP; blue: DAPI). Bars: 50 μm. *DM* diaphragmatic myoblasts, *MT* myotubes, *DMcx43* DM overexpressing connexin-43, *MTcx43* MT overexpressing connexin-43

relative expression of mRNA levels (Fig. 2d) of cx43 (2.63 ± 0.32 in DMcx43 vs. 1.00 ± 0.22 in non-transuced DMs, $p < 0.05$). While MTs derived from non-transduced DMs decreased its cx43 mRNA levels (MT: 0.21 ± 0.09), those derived from previously transduced DMs showed an increased cx43 expression (MTcx43: 9.22 ± 1.79).

With regard to cx43 protein expression (Fig. 2e, f), DMs (both transduced and non-transduced) showed a pattern similar to that of cx43 mRNA expression, i.e., higher for DMcx43 than for DM ($1.25 \pm 1.3 \times 10^{-1}$ vs. $1.0 \pm 3.2 \times 10^{-2}$, respectively, $p < 0.05$). In non-transduced MTs, cx43 protein levels were almost undetectable (as was observed for cx43 mRNA in this

group). Conversely, in cx43-transduced MTs the level of cx43 protein was much lower than expected from cx43 mRNA abundance. However, the difference in cx43 protein levels between MTcx43 and MTs was significant (MTcx43: $0.09 \pm 2.2 \times 10^{-2}$; MT: $0.01 \pm 3.4 \times 10^{-3}$, $p < 0.01$).

Cell viability (Fig. 2g) was not affected by the genetic modification (DM: $100.00 \pm 2.26\%$ and DMcx43: $95.55 \pm 9.67\%$; $p = NS$).

Figure 2h shows representative images of anti cx43 immunostaining in DMs transduced with Lv. pCMV/CX43iresGFP.

Assessment of cx43 gap junction coupling through FRAP of calcein-AM

Figure 3 shows FRAP-determined gap junction coupling due cx43 overexpression. Eight cells from four DMs and DMcx43 independent cultures were selected, ensuring that each cell was in contact with 2 or 3 cells in a similar position. Representative data show clear differences in recovery percentage and recovery rate (k) between DM and DMcx43 (Fig. 3b, c). In DMcx43 the photobleached region recovered was ~ 75% of the initial fluorescence while it was ~ 65% in DM cells (unpaired t test, $p < 0.05$). In addition, the recovery rate (Fig. 3c) obtained was significantly higher in DMcx43 cells with respect to DM cells (DM: 0.076 ± 0.010 vs. DMcx43: 0.108 ± 0.008, unpaired t test, $p < 0.05$). These results confirm that recombinant cx43 is functional, increasing gap junction coupling in transduced diaphragmatic myoblasts.

PLLA scaffolds characterization

Electrospun nanofibrous scaffolds with different fiber orientations were obtained (Fig. 4 and supplementary Fig. 2). The use of a rotating mandrel as collector allowed aligning the nanofibers along its circumferential direction. Different rotation speeds were tested, and an improvement in fiber orientation was observed as the speed increased. The nanofibers angle for random scaffolds was $92.00° \pm 53.37°$ (Fig. 4a, b). All the scaffolds produced with the rotating collector presented a lower standard deviation, indicating a better alignment of the fibers: $r1 = 91.96° \pm 37.50°$, $r2 = 96.33° \pm 31.17°$, $r3 = 94.98° \pm 28.55°$ (Fig. 4d, e and supplementary Fig. 2). Even though no

significant differences were found between diverse rotational speeds, a clear tendency could be observed both in the micrographs and unimodal histograms.

Then, we worked with non-aligned and aligned nanofiber scaffolds obtained at 1175 rpm (r3). As shown in Fig. 4c, f, the speed of rotation did not cause variations in fiber diameter (FD) [FD in random scaffold: 463 ± 131 nm vs. FD in aligned scaffold (r3): 468 ± 173, $p = NS$].

The processing technology influenced the thermal properties of random and aligned PLLA, decreasing the scaffold crystallinity with respect to the raw material. No differences were observed in the glass transition or the melting temperature. However, cold crystallization occurred on the electrospun samples. The thermal events and properties of random and aligned scaffolds did not show significant changes with the orientation (Table 1).

Morphological and cellular viability analysis on PLLA scaffolds

DMcx43 attached to PLLA scaffolds assumed different morphologies when interacting with random or aligned scaffolds (Fig. 5). Cells seeded on random nanofibers were attached to the scaffolds without specific orientation. Conversely, cells cultured on aligned scaffolds adopted an elongated morphology in the same direction of the nanofibers. Given that random and aligned scaffolds presented similar fiber diameter (Fig. 4c, f), the observed differences in cell morphology can be attributed to the different topography.

Cytoplasm orientation angles of DMcx43 seeded on random scaffolds (Fig. 6a) presented a wide distribution ($82.26° \pm 52.68°$), indicating a high disparity in cell elongation. By contrast, cells seeded on aligned scaffolds (Fig. 6b) showed narrow distribution of cell orientation angles ($88.52° \pm 17.13°$), indicating that cells remained oriented in the main direction of the nanofibers after 4 days in culture.

Cell viability for both DMs and DMcx43 was equal when seeded on PLLA aligned scaffolds or on glass disks after 4 days in culture (DM-Glass: $100 \pm 3.57\%$ vs. DMcx43-Glass: $99.09 \pm 9.50\%$ vs. DM-PLLA: $102.27 \pm 3.58\%$ vs. DMcx43-PLLA: $98.06 \pm 5.05\%$, $p = NS$). (Fig. 6c).
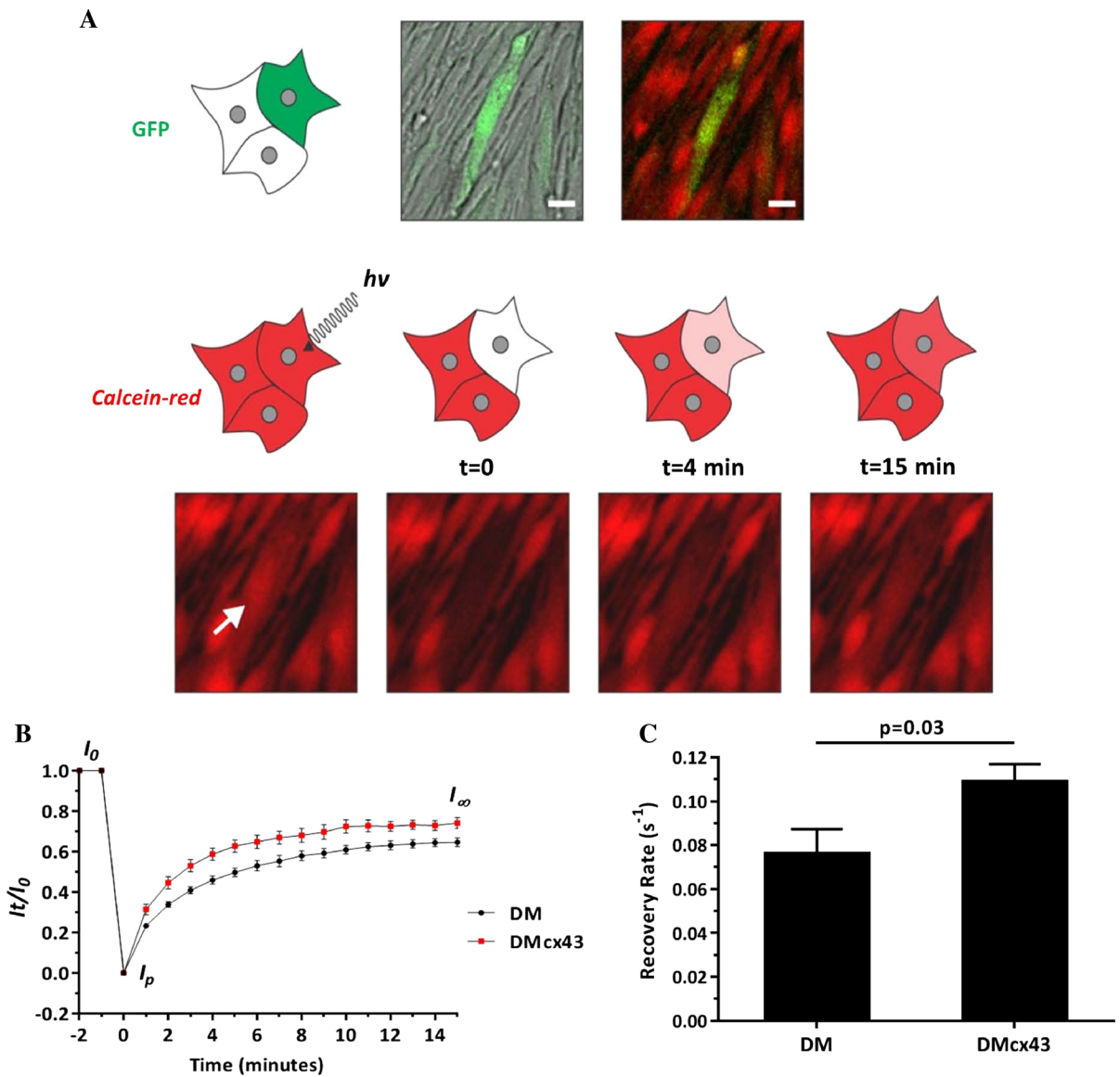
Fig. 3 Fluorescence recovery after photobleaching (FRAP). **a** Upper panel: Representative diaphragmatic myoblasts transduced with connexin-43 stained with calcein-red in culture for FRAP experiment. Lower panel: images show over time color recovery of the selected cell (arrow) after photobleaching. **b** Color recovery curves (mean ± SEM at different time points) for diaphragmatic myoblasts and diaphragmatic myoblasts transduced with connexin-43. Higher recovery of intensity in diaphragmatic myoblasts transduced with connexin-43 at each time point can be observed (* $p < 0.05$, unpaired t-test). **c** Recovery rate (k) for transduced and non-transduced diaphragmatic myoblasts ($p = 0.03$, unpaired t-test). Bars: 20 μm. *DM* diaphragmatic myoblasts, *DMcx43* DM overexpressing connexin-43

Discussion

Skeletal myoblasts differ according to the muscle from which they are extracted. We selected diaphragmatic myoblasts for their unique characteristics described above, that make them potential candidates for cardio-regenerative strategies. Sample obtention required a minimally invasive procedure with no complications, and cell isolation, culture and characterization was straightforward, yielding homogeneous cell populations.
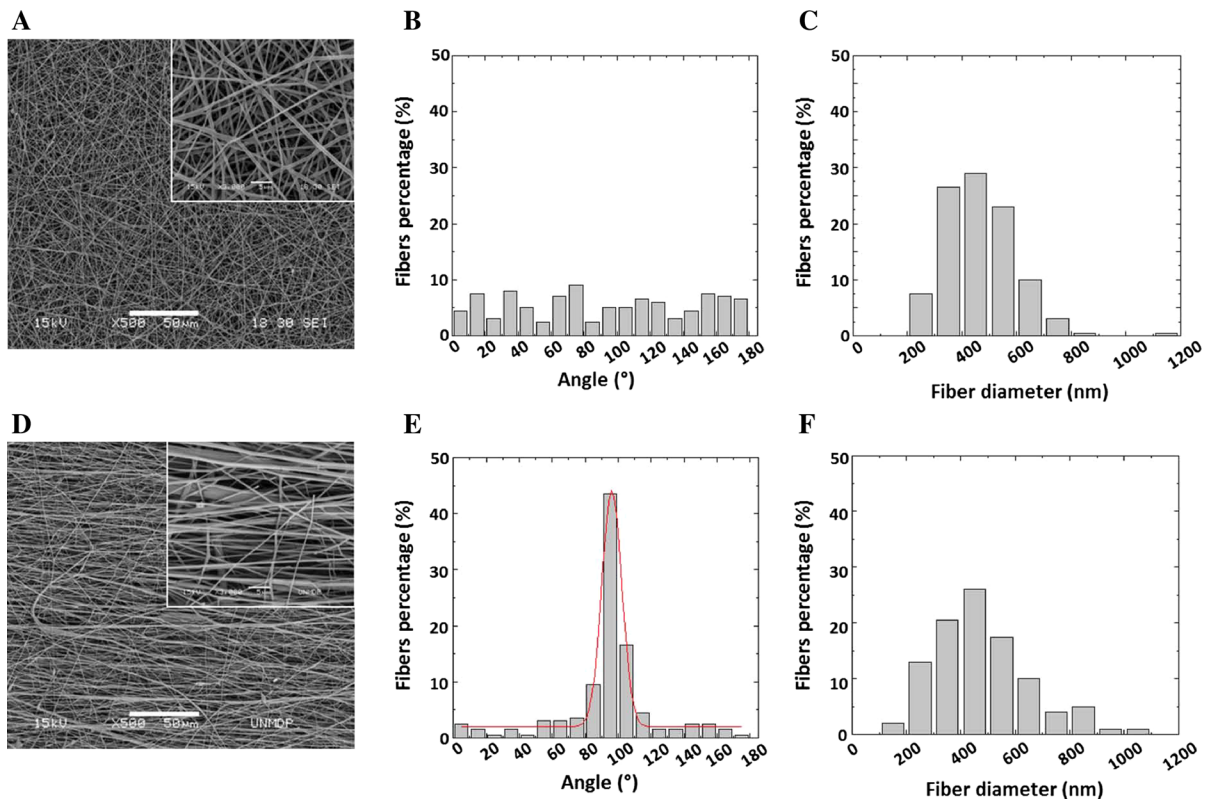
Fig. 4 Nanofiber topography analysis. a–c Scanning electron micrography (a), fiber alignment (b) and fiber diameter (c) in random poly (L-lactic acid) scaffolds. d–f Scanning electron micrography (d), fiber alignment (e) and fiber diameter (f) in aligned poly (L-lactic acid) scaffolds at 1175 rpm. Please note that the difference in topography of scaffolds with aligned nanofibers (d) corresponds to a higher percentage of fibers with the same alignment angle (e) in contrast to what it is observed in random scaffolds (a and b). The same pattern in fiber diameter distribution was observed in aligned and non-aligned scaffolds (c and f). Bars: 50 μm

Table 1 Thermal events and properties of random and aligned scaffolds

Scaffold	Tg (°C)	Tc (°C)	ΔHc (J/g)	Tm (°C)	ΔHm (J/g)	Xc (%)[a]
PLLA raw	61.4	–	–	152.5	35	37.6
PLLA random	61.6	82.06	14.6	153.4	35.4	22.3
PLLA r = 1175 rpm	61.4	86.5	11.2	154.4	34.4	24.9

Glass transition (Tg), crystallization (Tc), and melting (Tm) temperatures, crystallization (ΔHc), and melting (ΔHm) heats, and crystallinity degree (Xc) for the raw PLLA and PLLA electrospun scaffolds

[a] Degree of crystallinity values were calculated as $Xc = ((\Delta Hm - \Delta Hc) / \Delta Hm 100\%) \times 100$, where ΔHm100% is the crystallization heat for pure high molecular weight PLLA 100% crystalline considered as 93 J/g (Fischer et al. 1973)

Recent studies in vitro and on large mammalian models have shown that in myoblasts of skeletal muscles used in cardiac regeneration cx43 expression exerts an anti-arrhythmic effect by promoting electrical connectivity between implanted and resident cells (Fernandes et al. 2009; Greener et al. 2012). In the present study, we used a lentiviral vector to genetically modify DMs with the cx43 gene. These vectors are able to integrate stably into the genome of the transduced cells. We observed that myotubes differentiating from non-transduced DMs showed almost undetectable levels of cx43 mRNA.
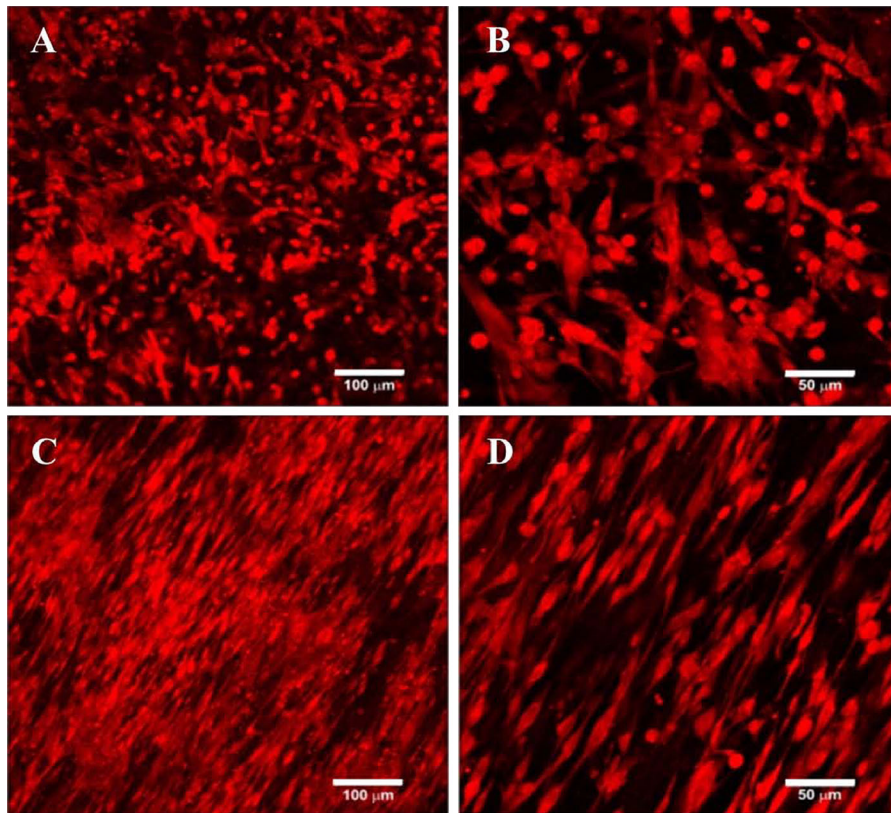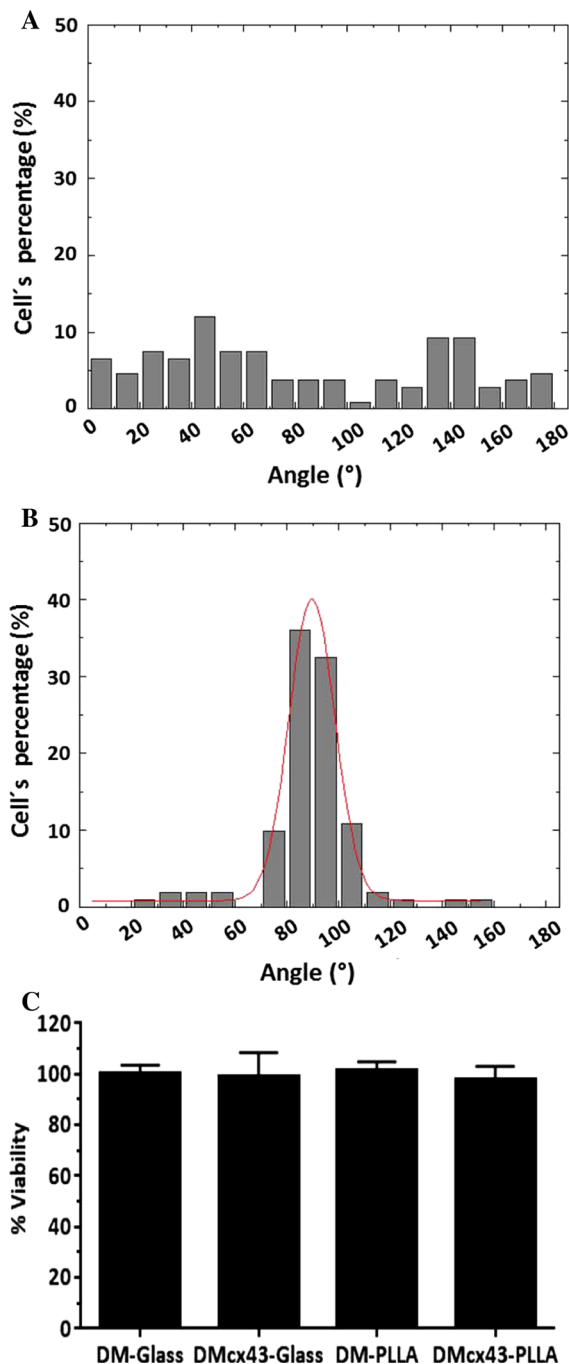
Fig. 5 Cell growth on poly (L-lactic acid) scaffolds. PKH26 red staining of diaphragmatic myoblasts grown on random (**a**, **b**), and aligned (**c**, **d**) poly (L-lactic acid) scaffolds after 4 days in culture. Image **a, c** Bars: 100 μm. Image **b, d**: Bars: 50 μm

Conversely, myotubes differentiating from cx43-transduced DMs exhibited levels of cx43 mRNA expression significantly higher than those of non-transduced DMs and also of cx43 transduced DMs. Interestingly, MTs differentiating from both non-transduced and tranduced DMs showed low levels of cx43 protein expression, revealing a post-translational inhibition phenomenon. However, it is important to note that due to the use of a strong promoter in our vector, the levels of cx43 protein in MTs originating from transduced DMs was significantly higher than those of MTs differentiating from non-transduced DMs. FRAP analysis revealed increased gap junction coupling in transduced DMs, indicating that the rise in the levels of recombinant cx43 was functional.

In stem cell-based cardiac regeneration strategies, cell retention in the myocardium remains a challenge. It has been shown that 90% of the successfully injected cells disappear within a week. In this regard, the use of scaffolds is advantageous because it provides support to cell colonization, migration and proliferation, until it is reabsorbed, thus enhancing cell retention in the target tissue (Fernandes 2004; Vu et al. 2012). In addition, the orientation of the cells is of key relevance for tissue function. Reports based on the contact guidance theory explain that cellular migration is associated with chemical, structural and mechanical properties of the substratum (Borradori and Sonnenberg 1999; Abbott 2003). In this sense, different studies have assessed the capacity of aligned nanofibers for guiding cellular orientation (Kenar et al. 2010; Jia et al. 2014; Shalumon et al. 2015). Recently, it was demonstrated that myogenic differentiation of C2C12 cells on polydioxanone is sensitive to fiber alignment and that the effects of alignment on differentiation are mediated via α7β1 signaling. These data indicate substrate-dependent interactions between myoblasts and aligned scaffolds that alter levels of myogenic regulatory factor expression, suggesting that myoblast signaling on aligned scaffolds is different from that on random

compare the alignment of the nanofibers obtained at different velocity of the collector with non-aligned nanofibers of PLLA obtained in static collector. Here we show how the alignment of the fibers improves with increasing tangential velocity of the collector. This tendency agrees with reported studies, where it has been stated that nanofiber alignment in the circumferential direction happens when the tangential velocity at the collector surface exceeds the velocity at which the nanofibres approach the collector (Bonani et al. 2011). Moreover, a collector rotation speed above the linear velocity of 4 m/s is required for visible fiber alignment (Ercolani et al. 2015). All of our tested rotation speeds exceeded 4 m/s (r1 = 6.28 m/s, r2 = 9.42 m/s, r3 = 12.30 m/s). The differences in the thermal properties of random and aligned PLLA with the processing technology was due to the fast solvent evaporation of the solution in the electrospinning process, not giving time to the polymer chains to accommodate into the crystalline structures (Zong et al. 2002).

We also showed how fiber organization promoted orientation of DMcx43 through contact guidance. Cell morphology and alignment in random and aligned scaffolds was different. In agreement with previous reports, these differences can only be attributed to the different topography, on account that both scaffolds presented similar fiber diameter and chemical properties (Whited and Rylander 2014).

In conclusion, our results show that diaphragmatic myoblasts, a kind of stem cells displaying features that make them potentially suitable for cardiac regeneration strategies, can be easily isolated and grown on PLLA scaffolds. Transduction of the cells with lentiviral vectors encoding the connexin-43 transgene favors intercell connectivity. Alignment

scaffolds (McClure et al. 2016). It has also been reported that aligned PLLA nanofibers can regulate the orientation of adhered cells and greatly influence cell growth and related functions (Díaz-Gómez et al. 2015). For these reasons, we decided to develop PLLA scaffolds by electrospinning technique and

of the scaffold fibers elongates and aligns the cells, increasing contact surface between cells, which, in turn, may contribute to increased connectivity. Future studies on animal models of myocardial infarction are needed to establish the usefulness of this approach on scar reduction and cardiac function.

Compliance with ethical standards

Conflict of interest The authors have no conflicts of interest to disclose.

References

Abbott A (2003) Cell culture: biology's new dimension. Nature 424:870–872

Abraham MR, Henrikson CA, Tung L, Chang MG, Aon M, Xue T et al (2005) Antiarrhythmic engineering of skeletal myoblasts for cardiac transplantation. Circ Res 97:159–167

Baroffio A, Bochaton-Piallat ML, Gabbiani G, Bader CR (1995) Heterogeneity in the progeny of single human muscle satellite cells. Differentiation 59:259–268

Beachley V, Wen X (2010) Polymer nanofibrous structures: fabrication, biofunctionalization, and cell interactions. Prog Polym Sci 35:868–892

Beauchamp JR, Morgan JE, Pagel CN, Partridge TA (1999) Dynamics of myoblast transplantation reveal a discrete minority of precursors with stem cell–like properties as the myogenic source. J Cell Biol 144:1113–1122

Bonani W, Maniglio D, Motta A, Tan W, Migliaresi C (2011) Biohybrid nanofiber constructs with anisotropic biomechanical properties. J Biomed Mater Res Part B Appl Biomater 96:276–286

Borradori L, Sonnenberg A (1999) Structure and function of hemidesmosomes: more than simple adhesion complexes. J Invest Dermatol 112:411–418

Delmar M, Makita N (2012) Cardiac connexins, mutations and arrhythmias. Curr Opin Cardiol 27:236–241

Díaz-Gómez L, Ballarin FM, Abraham GA, Concheiro A, Alvarez-Lorenzo C (2015) Random and aligned PLLA: PRGF electrospun scaffolds for regenerative medicine. J Appl Polym Sci http://onlinelibrary.wiley.com/doi/10.1002/app.41372/abstract

Dib N, McCarthy P, Campbell A, Yeager M, Pagani FD, Wright S et al (2005) Feasibility and safety of autologous myoblast transplantation in patients with ischemic cardiomyopathy. Cell Transplant 14:11–19

Ercolani E, Del Gaudio C, Bianco A (2015) Vascular tissue engineering of small-diameter blood vessels: reviewing the electrospinning approach. J Tissue Eng Regen Med 9:861–888

Farnsworth NL, Hemmati A, Pozzoli M, Benninger RKP (2014) Fluorescence recovery after photobleaching reveals regulation and distribution of Cx36 gap junction coupling within mouse islets of langerhans. J Physiol 592:4431–4446

Fernandes S (2004) Myocardial tissue engineering: creating a muscle patch for a wounded heart. Ann NY Acad Sci 1015:312–319

Fernandes S, Amirault JC, Lande G, Nguyen JM, Forest V, Bignolais O et al (2006) Autologous myoblast transplantation after myocardial infarction increases the inducibility of ventricular arrhythmias. Cardiovasc Res 69:348–358

Fernandes S, van Rijen HV, Forest V, Evain S, Leblond AL, Mérot J et al (2009) Cardiac cell therapy: overexpression of connexin43 in skeletal myoblasts and prevention of ventricular arrhythmias. J Cell Mol Med 13:3703–3712

Fischer E, Sterzel H, Wegner G (1973) Investigation of the structure of solution grown crystals of lactide copolymers by means of chemical reactions. Kolloid-ZuZ Polymere 251:980–990

Greener ID, Sasano T, Wan X, Igarashi T, Strom M, Rosenbaum DS et al (2012) Connexin43 gene transfer reduces ventricular tachycardia susceptibility after myocardial infarction. J Am Coll Cardiol 60:1103–1110

Gupta B, Revagade N, Hilborn J (2007) Poly (lactic acid) fiber: an overview. Prog Polym Sci 32:455–482

He X, Xiao Q, Lu C, Wang Y, Zhang X, Zhao J et al (2014) Uniaxially aligned electrospun all-cellulose nanocomposite nanofibers reinforced with cellulose nanocrystals: scaffold for tissue engineering. Biomacromol 15:618–627

Jia L, Prabhakaran MP, Qin X, Ramakrishna S (2014) Guiding the orientation of smooth muscle cells on random and aligned polyurethane/collagen nanofibers. J Biomater Appl 29:364–377

Kai D, Jin G, Prabhakaran MP, Ramakrishna S (2013) Electrospun synthetic and natural nanofibers for regenerative medicine and stem cells. Biotechnol J 8:59–72

Kenar H, Kose GT, Hasirci V (2010) Design of a 3D aligned myocardial tissue construct from biodegradable polyesters. J Mater Sci Mater Med 21:989–997

Lee J, Yim YS, Ko SJ, Kim DG, Kim CH (2011) Gap junctions contribute to astrocytic resistance against zinc toxicity. Brain Res Bull 86:314–318

Liu Q, Tian S, Zhao C, Chen X, Lei I, Wang Z et al (2015) Porous nanofibrous poly(L-lactic acid) scaffolds supporting cardiovascular progenitor cells for cardiac tissue engineering. Acta Biomater 26:105–114

Lopes MS, Jardini AL, Filho RM (2012) Poly (Lactic Acid) production for tissue engineering applications. Procedia Eng 42:1402–1413

McClure MJ, Clark NM, Hyzy SL, Chalfant CE, Olivares-Navarrete R, Boyan BD, Schwartz Z (2016) Role of integrin α7β1 signaling in myoblast differentiation on aligned polydioxanone scaffolds. Acta Biomater 39:44–54

Menasché P, Hagège AA, Vilquin JT, Desnos M, Abergel E, Pouzet B et al (2003) Autologous skeletal myoblast transplantation for severe postinfarction left ventricular dysfunction. J Am Coll Cardiol 41:1078–1083

Menasché P, Alfieri O, Janssens S, McKenna W, Reichenspurner H, Trinquart L et al (2008) The myoblast autologous grafting in ischemic cardiomyopathy (MAGIC) trial. First randomized placebo-controlled study of myoblast transplantation. Ciculation 117:1189–1200

Montini Ballarin F, Caracciolo PC, Blotta E, Ballarin VL, Abraham GA (2014) Optimization of poly(L-lactic acid)/segmented polyurethane electrospinning process for the production of bilayered small-diameter nanofibrous tubular structures. Mater Sci Eng C 42:489–499

Redshaw Z, McOrist S, Loughna P (2010) Muscle origin of porcine satellite cells affects in vitro differentiation potential. Cell Biochem Funct 28:403–411

Reneker DH, Yarin AL, Zussman E, Xu H (2007) Electrospinning of nanofibers from polymer solutions and melts. Adv Appl Mech 41:343–346

Sepúlveda DE, Cabeza Meckert P, Locatelli P, Olea FD, Pérez NG, Pinilla OA et al (2016) Activated macrophages as a feeder layer for growth of resident cardiac progenitor cells. Cytotechnology 68:665–674

Shalumon KT, Deepthi S, Anupama MS, Nair SV, Jayakumar R, Chennazhi KP (2015) Fabrication of poly (L-lactic acid)/gelatin composite tubular scaffolds for vascular tissue engineering. Int J Biol Macromol 72:1048–1055

Siminiak T, Kalawski R, Fiszer D, Jerzykowska O, Rzeźniczak J, Rozwadowska N et al (2004) Autologous skeletal myoblast transplantation for the treatment of postinfarction myocardial injury: phase I clinical study with 12 months of follow-up. Am Heart J 148:531–537

Sutton MG, Sharpe N (2000) Left ventricular remodeling after myocardial infarction: pathophysiology and therapy. Circulation 101:2981–2988

Suzuki K, Brand NJ, Allen S, Khan MA, Farrell AO, Murtuza B et al (2001) Overexpression of connexin 43 in skeletal myoblasts: relevance to cell transplantation to the heart. J Thorac Cardiovasc Surg 122:759–766

Vu DT, Martinez EC, Kofidis T (2012) Myocardial restoration: is it the cell or the architecture or both? Cardiol Res Pract 2012:240497. https://doi.org/10.1155/2012/240497

Whited BM, Rylander MN (2014) The influence of electrospun scaffold topography on endothelial cell morphology, alignment, and adhesion in response to fluid flow. Biotechnol Bioeng 11:184–195

Yarin AL, Zussman E (2004) Upward needleless electrospinning of multiple nanofibers. Polymer 45:2977–2980

Zong X, Kim K, Fang D, Ran S, Hsiao BS, Chu B (2002) Structure and process relationship of electrospun bioabsorbable nanofiber membranes. Polymer 43:4403–4412